This manuscript was accepted by J. Appl. Phys. Click here to see the version of record.

Interface-mediated ferroelectric patterning and Mn valency in nanostructured $PbTiO_3/La_{0.7}Sr_{0.3}MnO_3$

Ingo P. Krug,[1,2,3] Hatice Doganay,[1,4] Florian Nickel,[1,4] Daniel M. Gottlob,[1,4] Claus M. Schneider,[1,5,6] Alessio Morelli,[7,8] Daniele Preziosi,[7,9,10] Ionela Lindfors-Vrejoiu,[7,11,12] Robert Laskowski,[13,14] and Nick Barrett[4]

[1)] *Peter Grünberg Institut (PGI-6), Forschungszentrum Jülich, DE-52425, Germany*

[2)] *Institut für Optik and Atomare Physik (IOAP), Technische Universität Berlin, DE-10623 Berlin, Germany*

[3)] *Helmholtzzentrum für Materialien und Energie (HZB), DE-12489 Berlin, Germany*

[4)] *SPEC, CEA, CNRS, Université Paris-Saclay, CEA Saclay 91191 Gif-sur-Yvette Cedex, France*

[5)] *JARA Jülich-Aachen Research Alliance, Forschungszentrum Jülich, DE-52425 Jülich, Germany*

[6)] *Fakultät für Physik and Center for Nanointegration Duisburg-Essen (CeNIDE), DE-47048 Duisburg, Germany*

[7)] *Max Planck Institute of Microstructure Physics, DE-06120 Halle, Germany*

[8)] *Centre for Nanostructured Media, School of Mathematics and Physics, Queen's University Belfast, University Road, Belfast BT7 1NN, Northern Ireland, UK*

[9)] *Unité Mixte de Physique CNRS/Thales, 1 avenue A. Fresnel, 91767 Palaiseau, France*

[10)] *Université Paris-Sud, 91405 Orsay, France*

[11)] *Max Planck Institute for Solid State Research, DE-70569 Stuttgart, Germany*

[12)] *II. Physikalisches Institut, Universität zu Köln, 50937 Cologne, Germany*

[13)] *Institute of Materials Chemistry, Vienna University of Technology, A-1060 Vienna, Austria*

[14)] *Materials Science & Engineering Department Institute of High Performance Computing, A*STAR 1, Fusionopolis Way, #16-16, Connexis, Singapore 138632*

We employed a multitechnique approach using piezo-force response microscopy and photoemission microscopy to investigate a self-organizing polarization domain pattern in $PbTiO_3/La_{0.7}Sr_{0.3}MnO_3$ nanostructures. The polarization is correlated with the nanostructure morphology as well as with the thickness and Mn valence of the LSMO template layer. On the LSMO dots the PTO is upwards polarized whereas outside the nanodots the polarization appears both strain and interface roughness dependent. The results suggest that the electronic structure and strain of the PTO/LSMO interface contribute to determining the internal bias of the ferroelectric layer.

PACS numbers: 68.37.-d, 77.80.-e, 75.85.+t

I. INTRODUCTION

In ferroelectric thin films, the preferred orientation of the polarization, termed *ferroelectric internal bias*[1,2] is at the origin of the so-called *imprint* effect. On the one hand, the imprint may destabilize the ferroelectric state and promote fatigue[2,3] over time and with the number of switching cycles. On the other hand, if it is carefully tailored and pre-engineered into the system, it can help to improve device switching speeds[4]. Importantly, for spintronics and memory applications, it can also be used to create patterned ferroelectric storage media[5], or even artificial multiferroics[6–9] when combined with magnetic materials.

Ferroelectric internal bias manifests itself as a shift of the hysteresis loop along both the electric field and the polarization axes, i.e. the ferroelectric polarization is pinned in one direction. Asymmetric space charge at the upper or lower interface of a thin film will directly favor one polarization state over the other via the built-in electric field[10,11]. The origin of the space charge can be manifold, for example, trapped charges due to the presence of ferroelectrically dead layers at the interfaces[12,13], charge-transfer[14–16] dipole moments at electrically asymmetric interfaces[17,18], or migration of charged defects inside the layer by internal or external electric fields[1,2]. As an example for interface chemistry, different imprint states occur for *as-grown* $PbZr_{0.2}Ti_{0.8}O_3$ (PZT) deposited on either $SrRuO_3$ (outward, P^+) or $La_{0.7}Sr_{0.3}MnO_3$ (inward, P^-)[14].

Nanostructures can be particularly sensitive to the ferroelectric imprint. In nanostructured PTO/LSMO similar to the present study the thickness of the LSMO layer determines the location of 180° domain walls[19]. Internal bias can couple with charge ordering at the PTO/LSMO interface[20].

Here we employ photoemission electron microscopy using soft x-rays (X-PEEM) to study the ferroelectric imprint and Mn valency at the PTO/nanostructured LSMO buried interface in a spatially resolved manner. X-PEEM has already been successfully used to study ferro- and antiferromagnetic domains as well as ferroelectrics[21–23] and multiferroics[24,25].

The spectroscopic signature of the *out-of-plane* ferro-

electric state in our samples was characterized following the approach of Arenholz *et al.*[14], measuring the polarity-dependent fine structure at the Ti $L_{2,3}$-edges. The Mn L-edges yield information about the Mn valence state in LSMO which is crucial for its electrical and magnetic properties. Piezo-response force microscopy (PFM) was used to map the ferroelectric polarization. Contrary to Arenholz *et al.* [14], the PTO is upwards polarized on the thick LSMO nanodots, possibly because of the nanostructured shape and interface roughness. Outside the dots the polarization appears to depend on the LSMO roughness and strain.

II. EXPERIMENT

The samples were prepared by pulsed laser deposition (PLD). Details about the preparation of similar systems can be found in Ref.[26]. **First, a $La_{0.7}Sr_{0.3}MnO_3$ dot pattern was deposited on a (001)-oriented Nb-doped $SrTiO_3$-substrate (STON) at 600 °C in 0.028 mbar O_2 through a SiN stencil mask using 10000 laser pulses at 5 Hz. Then, the sample was cooled down at -10°C/min in 700 mbar O_2. The stencil mask was removed, the sample was reintroduced into the chamber and heated to 130 °C, then exposed to 5 mbar O_2, then heated to 585 °C and kept the sample for 30 minutes at that temperature. Then, a continuous ferroelectric $PbTiO_3$ top-layer of 4 nm thickness was grown on top of the dots at a temperature of 585 °C using 180 laser pulses at 3 Hz (see Fig. 1(a)). The sample was allowed once more to cool down in 700 mbar O_2. The whole structure is shown schematically in Fig 1(a).** The low thickness was chosen to exalt the role of the interfaces with respect to that of the bulk film.

Atomic force microscopy (AFM) measured an LSMO dot height of 37 nm in the center of the dots **(see Fig 1(b))**. The LSMO between the dots stems from shadowing which occurs during the plasma-dynamics of the PLD process, favored by incomplete contact of the mask. In our case this is useful since it also allows to study PTO on thin LSMO. The LSMO thickness between the dots is 1-2 nm, as estimated by XAS measurements.

PFM[27] as shown in Fig. 1(c) reveals that a self-organized polarization pattern forms spontaneously, with the ferroelectric polarity pointing upwards (P^+) on top of the dots and also in a large area fraction between the dots (85% upwards polarization in total). A small fraction (15 %) of the surface, however, consists of a regular array of downwards (P^-) polarized, crescent moon regions, as shown in Fig. 1(c) and (d), at the maximum distance possible from the dot centers. The AFM topography shows that in these regions the LSMO surface has the lowest roughness, whereas in the dot regions, the higher LSMO thickness leads to roughening of the LSMO and the PTO overlayer (see Fig. 2). For the exterior P^+ regions, the rms roughness is 0.23 nm whereas for P^- it is only 0.18 nm.

FIG. 1. (color online) a) Sample layout: LSMO dots are deposited by a stencil mask onto a STON substrate. Due to shadowing, the dots exhibit a smooth LSMO thickness gradient at their edges. A 4 nm PTO layer is deposited on top. b) AFM topography: Peak height of the dots is about 37 nm. c) PFM phase image. The dots and a large fraction of the exterior are outwards polarized (P^+), in between there exist crescent-shaped areas with downwards (P^-) polarization. d) Sketch of the polarity pattern.

X-PEEM using soft X-rays was performed using a SPECS P90 FE aberration-corrected LEEM-PEEM at the UE56-1 SGM beamline, BESSY II, Helmholtz-Zentrum (Berlin). The photon incidence angle is 20 °. All measurements were done at room temperature. The instrument comprises an in-line energy filter which was set to 3 eV bandwidth and operated in secondary electron yield mode (SEY). For XAS the electron kinetic energy was set to maximum SEY intensity and image series were acquired as a function of the incident photon energy.

FIG. 2. (color online) a) Topography, small scan area in between the dots with enhanced height resolution. b) Horizontal Sobel filtering shows the different correlation lengths of the surface roughness. The crescent-shaped area of the regions outside the dots is much flatter than the rest of the sample. c) PFM phase contrast: Dark regions exhibit a P^- state.

III. RESULTS

A. Ti $L_{2,3}$ edge

The kinetic energy shift of the secondary electron peak is a measure of the local surface potential which may be correlated with the ferroelectric state[21,22]. The threshold image shown in Fig. 3 allows to define the regions for microspectroscopy by XAS.

FIG. 3. (color online). PEEM image with regions of interest for microspectroscopy.

In Fig. 4 we show the X-ray absorption measurements at the Ti L-edge for the external P^+ and P^- regions to highlight differences in spectral shape due to the ferroelectric polarity. In Fig. 4(a) the XAS spectra are shown for *p*- and *s*- light polarizations, i.e. where the **E**-vector is oriented *out-of-plane* and *in-plane*, respectively.

The tetragonal distortion splits the e_g into a high energy $(x^2 - y^2)$ level and low energy $(3z^2 - r^2)$ level, and the t_{2g} levels into a high (xy) and low energy (xz, yz) levels, producing pronounced X-ray linear dichroism (XLD) between *out-of-plane* and *in-plane* light polarization, as

This manuscript was accepted by J. Appl. Phys. Click here to see the version of record.

FIG. 4. (color online) Ti L-edge spectromicroscopy. a) Experimental and theoretical XAS spectra. (Blue) P^+, (Red) P^- polarized regions as shown in Fig. 1c). The theory curves correspond to two unit cell models with different crystalline structures representing the two ferroelectric surfaces. b) Comparison of experimental ($I_p - I_s$) and theoretical XLD ($I_\perp - I_{||}$). c) photon-polarization-averaged difference spectrum between P^+ and P^- sample areas, experiment and theory. **Remark: experimental and theory curves have been offset from 0, for clarity.**

shown in Fig. 4(b). In bulk PTO P^+ and P^- are mirror-symmetric therefore their XLD structures should be indistinguishable. Any difference must be due to a polarity-specific symmetry reduction at the layer *surface* or *interface*. The XLD for the P^+ state is slightly weaker than for P^-, as can be seen from the difference curve in Fig. 4(b), indicating an enhanced tetragonality for P^-.

FIG. 5. (color online) Mn L-edge spectra. Upper part: Reference spectra taken from[28]. In the bottom part of the graph, again spectra in the two regions from Fig. 1c) are shown. (red crescents/red dotted line: P^-, blue squares/line: P^+). In addition, the P^+ regions on the dots are shown (grey curve).

By averaging over *s*- and *p*-polarization, the effects of the FE polarity become more apparent (lower curve in Fig. 4(c)). The difference curve consists of three features which we label t_{2g}, e_gA and e_gB, equally present at the L_3 and L_2 edges **(see, for example inset in Fig. 4(a))**. For P^+, t_{2g} and e_gB increase while e_gA decreases. This behaviour agrees with the experimental findings of Arenholz *et al.*[14] who explained it in terms of an inward relaxation of the layer for P^+ and an outward relaxation for P^-, supported by atomic multiplet calculations[14].

To better understand the effect of ferroelectric distortion on the absorption spectra, we modelled the Ti L-edge spectra by solving the Bethe-Salpeter equation (BSE)[29]. The approach properly reproduces the branching ratio and also takes into account solid state effects, since it was shown by similar calculations that the e_g peak splitting is *not* a *local* effect[30,31], in contrast to atomic multiplet calculations used by Arenholz *et al.* which make only a *local* approximation. We apply this method to compute the XLD for the bulk phase of $PbTiO_3$ and to estimate the effect of variation of the ferroelectric polarization on the XLD.

Our *ab-initio* approach correctly reproduces most features of the measured XLD spectra. Since solving BSE is computationally very expensive it is not possible to apply it for any reasonable model of the surface. However, surface effects can be modelled by mimicking crystalline distortions of the surface unit cell. We used a bulk model reproducing "P^+ " (surface 2) and "P^- " (surface 1) structures at the sample surface.

The calculation for surface 2 resulted in an almost relaxed (cubic) phase whereas surface 1 corresponds to a strongly tetragonally distorted ferroelectric phase with downwards polarization (P^-).

The theory spectra are shown in Fig.4(a) and the difference is shown in Fig.4(c). Despite the crudeness of such an approach (P^+ is approximated by tetragonaly distorted paraelectric phase), the theory results are remarkably close to the experimental curve, showing that the PTO polarization state can be characterized by the spectral shape of the Ti L-edge XAS.

FIG. 6. (color online) . Polarization-averaged XAS spectra for comparison of 4 nm PTO on two different LSMO thicknesses (3 and 10 nm). Clearly, the low thickness sample shows a low energy peak at the L_3 edge which is not present in the thicker film. The difference curve resembles a MnO XAS spectrum in the low energy part, indicating that the Mn^{2+} valence is increased for thin films.

B. Mn $L_{2,3}$ edge

In Fig. 5, Mn L-edge spectra, measured through the 4 nm PTO overlayer, are shown for the exterior P^+, P^- and the P^+ dot polarizations as defined in Fig. 1. The Mn edge in the dots is shifted to higher energy than in the P^+ regions outside the dots. Following Vaz *et al.*[20] P^+ polarization should give rise to hole accumulation in both cases, however, the LSMO outside the dots is much thinner. The edge position outside the dots corresponds to hole-depleted LSMO, suggesting that the film thickness plays an important role.

The experimental spectra of the P^+ and P^- regions exhibit different L_3 lineshapes. By comparison with reference Mn oxide spectra reproduced from Ref. [28], we can assign the peak shapes to changes in the Mn valence state. The Mn^{2+} reference lineshape has been used to align the energy scales of experimental and reference spectra.

The exterior P^+ regions (blue curve) exhibit a strongly asymmetric lineshape with a low energy maximum. This peak almost coincides with the MnO reference spectrum indicating that there is a strong admixture of a Mn^{2+} valence state. Thus, the exterior P^+ regions correspond to LSMO with dominating Mn^{2+} valence state. Lower Mn valence states are improbable since they would correspond to underoxidized LSMO, unlikely in the PLD growth process.

In the exterior P^- regions, the peak positions match the Mn_2O_3 reference curve, suggesting a dominant contribution of the Mn^{3+} valence state. Mn_3O_4 ($Mn^{2+/3+}$) also has a peak at the same energy as the P^- spectra, but in addition a pronounced low energy peak which is characteristic of Mn^{2+}. From this we conclude that Mn^{3+} is dominant but no prominent Mn^{2+} is present in the crescent P^- regions.

The LSMO dots where the PTO polarity is also P^+, exhibit a spectrum with characteristic features for both

This manuscript was accepted by J. Appl. Phys. Click here to see the version of record.

Mn^{3+} and Mn^{4+}, indicating that the structure is closer to that of bulk LSMO and the Mn edge is shifted to higher energy.

Thus, in the LSMO layer, (i) the exterior P^- regions show mainly a Mn^{3+} valence state, while the exterior P^+ regions are dominated by Mn^{2+} valency. The LSMO in the exterior of the dots shows suppressed Mn^{4+} valence, while the LSMO in the dots shows almost a bulk Mn L-edge signature. The overall valency in the thin LSMO layer outside the dots is reduced as compared to both bulk LSMO and the LSMO dots. Below we discuss how space charge and electronic reconstruction can contribute to the Mn valence changes.

FIG. 7. (color online)X-ray Linear Dichroism for the Mn edge for different LSMO thicknesses. The 3 nm layer shows a substantially altered shape and increased amplitude of the XLD. The integrated XLD signal $I_p - I_s$ is negative, meaning that *in-plane*-orbitals are preferentially occupied.

XAS measurements were also done on uniform, non-nanostructured, LSMO layers of different thickness sandwiched between a 4 nm PTO layer at the top and the STON substrate at the bottom (Fig.6). We prepared a thick, 10 nm film, with negligible signal from the lower LSMO/STON interface, and a thin, 3 nm film, providing access to the complete LSMO layer including the lower interface.

The 3 nm layer exhibits a strong low-energy feature at the Mn L_3-edge near 639 eV, charactersitic of Mn^{2+}, missing in the thicker 10 nm film whereas the latter has a spectrum closely resembling that of Mn_2O_3 (3+). The pre-edge feature in the difference spectrum of Fig. 6 closely resembles a MnO spectrum, while the main peak feature with opposite sign resembles more the Mn_2O_3 spectrum as shown in the middle panel. The 3 nm film is therefore hole depleted with respect to the 10 nm film. This means that there is a valence shift from Mn^{3+} towards Mn^{2+} when going from the uniform 10 nm the 3 nm film. Similar behaviour has also been found by Valencia *et al.*[32] and electron energy loss spectroscopy identified this feature to be an interface effect[33,34]. In our nanostructured sample, the LSMO under the P^- regions is only 1-2 nm thick and therefore both interfaces, PTO/LSMO and LSMO/STO contribute to the Mn absorption edge structure.

There are several important results which can be deduced from the spatially resolved Ti and Mn $L_{2,3}$ absorption spectra. The PTO is P^+ polarized above the thick LSMO dots, giving rise to hole accumulation in the LSMO. The thin LSMO outside the dots is different. The PTO is P^+ polarized above slightly rougher LSMO and P^- polarized above the smoother LSMO (crescent shaped regions). The Ti $L_{2,3}$ edge has all the features of FE tetragonal phase of PTO. AFM results suggest a quite different strain state in the exterior P^+ and P^- regions. This may explain why the P^- polarization state reported by Arenholz *et al.* is only observed in the exterior crescent shaped regions.

The Mn valency changes not only with LSMO thickness but also as a function of the PTO polarization state. For very thin LSMO, the Mn is in general reduced with respect to that in bulk LSMO and underneath the P^+ and P^- regions the Mn has dominating 2+ and 3+ valence state, respectively.

IV. DISCUSSION

We now discuss the different interface-related mechanisms coupling the polarization imprint and the Mn valence states in this nano-structured geometry.

A. Space charge

We first consider charge transfer due to the built-in field between the n-type STON and the p-type LSMO. The LSMO and the STON form a p-n junction with electron accumulation on the LSMO side of the interface setting up a space charge region whose width is determined by the effective doping level of the LSMO. The carrier concentration for Nb(0.5 wt.%):STO is of the order of 10^{21} cm^{-3}, i.e. it is highly doped[35]. This means that the number of mobile electrons per unit cell can easily attain $\sim$0.1 to 1.0 e/u.c. Electrons crossing the lower interface into the LSMO can fill mobile holes in the Mn d-states, thereby reducing the effective valence state and creating *hole depletion* as observed in the thin LSMO. However, charge transfer of mobile carriers from the substrate setting up a space charge region is not necessarily the only mechanism responsible for the change in the XAS lineshape. Also, it is only valid for the bottom LSMO/STON interface.

B. Electronic reconstruction at the LSMO interfaces

Electronic reconstruction due to the polar discontinuity and associated *local* charge transfer at the upper and lower **interfaces** must also be considered. Since $La_{0.7}Sr_{0.3}MnO_3$ is a polar oxide, an electronic reconstruction similar to $LaAlO_3/SrTiO_3$[36] may occur at both the LSMO/PTO and the LSMO/STO interface, in order to screen the polar discontinuity. In an ideal picture, $1/3\,e^-$ or $1/3\,h$ per unit cell is transferred to the MnO_2 plane closest to the interface, depending on the termination[37]. There are two possible interfaces: i) MnO_2-$La_{0.7}Sr_{0.3}O$-TiO_2-SrO (n-type interface) and ii) $La_{0.7}Sr_{0.3}O$-MnO_2-SrO-TiO_2 (p-type interface). On TiO_2 terminated STO, as in our case, the first layer in the LSMO should be $La_{0.7}Sr_{0.3}O$, i.e. an n-type interface and the MnO_2 plane nearest to the interface should receive $1/3\,e^-$ to avoid the polar catastrophe. In reality, interfacial cation intermixing and oxygen vacancy formation are additional mechanisms to be considered, but are beyond the scope of

our paper. We suggest, however, that the interface electronic reconstruction may be partly responsible for the Mn valence change. Other studies, for example Mundy *et al.*, assign a Mn^{2+} contribution to the LSMO/STO interface[38].

Besides this, at the PTO/LSMO interface, additional charge must be screened due to the FE polarization of PTO. Such changes should be reflected in the XAS spectra of regions with opposite polarity, but of equal LSMO thickness. Chen *et al.* predicted that by switching the ferroelectric polarization, the LSMO hole doping can be changed from 0 $\frac{h}{Mn}$ (depletion or P^-) to almost 1 $\frac{h}{Mn}$ (accumulation, P^+) in the MnO_2 plane closest to the interface[15]. Experiments with hard x-ray absorption on PZT/LSMO nanocapacitors support this hypothesis. Vaz *et al.* found that a a chemical shift of the Mn K-edge is associated with polarization reversal of a PZT layer in contact with LSMO[20]. Here, the Mn absorption edge in the hole-depleted state (P^-) is at higher energy. However, as shown by the Mn edges in Fig.5 and Fig.6, the LSMO thickness appears to play an important role in determining the hole depletion/accumulation. This effect requires more study since LSMO also loses its metallicity in very thin layers[37,39,40].

C. LSMO orbital ordering and PTO polarization

In addition to the effect of the built-in field and of polarization-induced variations in doping we must also consider the role of the local chemistry and bond hybridization at the PTO/LSMO interface. Fig. 7 shows the XLD spectra for the 3 and $d = 10$ nm LSMO layers sandwiched between a STON substrate and a 4 nm PTO layer.

For the 10 nm layer, the XLD is small and slightly positive, indicating preferential *out-of-plane* orbital ordering of electrons, whereas for the thinnest layer of $d = 3$ nm thickness, the XLD becomes considerably stronger, changes its shape, with its integral being negative. In conclusion, the *in-plane* orbitals are preferentially occupied for the thinner LSMO.

The shape of the XLD in the thin LSMO layer closely resembles the spectrum of a thin $LaMnO_3$(3 u.c.)/STO(2 u.c.) superlattice[41]. The authors of this study argue that interfacial distortion/charge transfer is responsible for the spectral shape and sign of the XLD, with *in-plane* ordering of ultrathin LMO layers (3 u.c.) and *out-of-plane* ordering for thicker layers (17 u.c.).

We suggest that electronic *in-plane* orbital ordering of thin LSMO layers can lead to an altered charge balance of the PTO/LSMO interface, thereby facilitating the formation of a P^- state in the PTO, i.e. a positive fixed polarization charge at the PTO/LSMO interface. Alternatively, full depletion of the LSMO layer due to the junction with the n-type Nb-doped STO substrate may also provide a source of electronic charge to screen the positive polarization charge. Further work is necessary to elucidate this point.

V. CONCLUSION

In conclusion, independent measurements by PFM and XPEEM spectromicroscopy show that a PTO layer deposited on an LSMO nanostructured template spontaneously forms a polarity-domain pattern consisting of 180° *out-of-plane* polarized regions. The polarity pattern correlates with the LSMO thickness and roughness. Regions where the LSMO is thin show a reduced Mn valency, i.e. hole depletion. P^+-polarized regions exhibit a valence state shifted towards Mn^{2+} while P^--polarized regions show a spectrum closer to Mn^{3+}. Ultrathin LSMO layers sandwiched between the STON substrate and a PTO layer show *in-plane* orbital ordering of the Mn 3d electrons with an electronic reconstruction different from thicker LSMO layers. These correlations strongly suggest that a mix of electronic, structural and mechanical effects is at play: space charge, electronic reconstruction via charge transfer and orbital ordering combine to determine the local ferroelectric imprint. The latter is therefore the result of complex interactions between several competing electronic phenomena which must be fully understood in order to envisage engineering of novel ferroelectric based electronics. It is clear, for example, that the role of thickness dependent microstrain on the flexoelectric effect must be further studied. The results are of importance for the understanding of functional FE/FM heterointerfaces, concerning local imprint, magnetoelectric and transport properties[42].

ACKNOWLEDGMENTS

We thank HZB for the allocation of synchrotron radiation beamtime. We thank O. Schaff and A. Kaiser from SPECS as well as R. Tromp for valuable discussions and support with the LEEM-PEEM instrument. We acknowledge the help and valuable discussions with J. Wang, as well as S. Cramm for beamline support.

[1] G. Arlt and H. Neumann, Ferroelectrics **87**, 109 (1988).
[2] D. Damjanovic, Reports on Progress in Physics **61**, 1267 (1998).
[3] M. Dawber and J. F. Scott, Applied Physics Letters **76**, 1060 (2000).
[4] Y. Hou, Z. Lü, T. Pu, Y. Zhang, G. Xu, and H. Xu, Applied Physics Letters **102**, 063507 (2013).
[5] H.-J. Shin, J. H. Choi, H. J. Yang, Y. D. Park, Y. Kuk, and C.-J. Kang, Applied Physics Letters **87**, 113114 (2005).
[6] R. V. Chopdekar and Y. Suzuki, Applied Physics Letters **89**, 182506 (2006).
[7] Y. Zhang, Journal of Applied Physics **92**, 152510 (2008).
[8] R. V. Chopdekar, V. K. Malik, A. Fraile Rodriguez, L. Le Guyader, Y. Takamura, A. Scholl, D. Stender, C. W. Schneider, C. Bernhard, F. Nolting, and L. J. Heyderman, Phys. Rev. B **86**, 014408 (2012).

[9] L. Jiang, W. S. Choi, H. Jeen, S. Dong, Y. Kim, M.-G. Han, Y. Zhu, S. V. Kalinin, E. Dagotto, T. Egami, and H. N. Lee, Nano Letters **13**, 5837 (2013).
[10] I. B. Misirlioglu, M. B. Okatan, and S. P. Alpay, Journal of Applied Physics **108**, 034105 (2010).
[11] I. Misirlioglu, M. Okatan, and S. Alpay, Integrated Ferroelectrics **126**, 142 (2011).
[12] M. Grossmann, O. Lohse, D. Bolten, U. Boettger, T. Schneller, and R. Waser, Journal of Applied Physics **92**, 2680 (2002).
[13] M. Grossmann, O. Lohse, D. Bolten, U. Boettger, and R. Waser, Journal of Applied Physics **92**, 2688 (2002).
[14] E. Arenholz, G. van der Laan, A. Fraile-Rodríguez, P. Yu, Q. He, and R. Ramesh, Phys. Rev. B **82**, 140103 (2010).
[15] H. Chen and S. Ismail-Beigi, Phys. Rev. B **86**, 024433 (2012).
[16] T. Y. Chien, L. F. Kourkoutis, J. Chakhalian, B. Gray, M. Kareev, N. P. Guisinger, D. A. Muller, and J. W. Freeland, Nature Communications **4** (2013), 10.1038/ncomms3336.
[17] C.-G. Duan, R. F. Sabirianov, W.-N. Mei, S. S. Jaswal, and E. Y. Tsymbal, Nano Letters **6**, 483 (2006).
[18] P. Yu, W. Luo, D. Yi, J. X. Zhang, M. D. Rossell, C.-H. Yang, L. You, G. Singh-Bhalla, S. Y. Yang, Q. He, Q. M. Ramasse, R. Erni, L. W. Martin, Y. H. Chu, S. T. Pantelides, S. J. Pennycook, and R. Ramesh, Proceedings of the National Academy of Sciences **109**, 9710 (2012).
[19] L. Jin, C. L. Jia, and I. Vrejoiu, Applied Physics Letters **105**, 132903 (2014).
[20] C. A. F. Vaz, J. Hoffman, Y. Segal, J. W. Reiner, R. D. Grober, Z. Zhang, C. H. Ahn, and F. J. Walker, Physical Review Letters **104**, 127202 (2010).
[21] I. Krug, N. Barrett, A. Petraru, A. Locatelli, T. O. Mentes, M. A. Niño, K. Rahmanizadeh, G. Bihlmayer, and C. M. Schneider, Applied Physics Letters **97**, 222903 (2010).
[22] N. Barrett, J. Rault, I. Krug, B. Vilquin, G. Niu, B. Gautier, D. Albertini, P. Lecoeur, and O. Renault, Surface and Interface Analysis , DOI: 10.1002/sia.3369 (2010).
[23] S. Polisetty, J. Zhou, J. Karthik, A. R. Damodaran, D. Chen, A. Scholl, L. W. Martin, and M. Holcomb, Journal of Physics: Condensed Matter **24**, 245902 (2012).
[24] T. Zhao, A. Scholl, F. Zavaliche, H. Zheng, M. Barry, A. Doran, K. Lee, M. P. Cruz, and R. Ramesh, Applied Physics Letters **90**, 123104 (2007).
[25] Y.-H. Chu, L. W. Martin, M. B. Holcomb, M. Gajek, S.-J. Han, Q. He, N. Balke, C.-H. Yang, D. Lee, W. Hu, Q. Zhan, P.-L. Yang, A. Fraile-Rodríguez, A. Scholl, S. X. Wang, and R. Ramesh, Nature Materials **7**, 478 (2008).
[26] I. Vrejoiu, A. Morelli, F. Johann, and D. Biggemann, Applied Physics Letters **99**, 082906 (2011).
[27] A. Gruverman, O. Kolosov, J. Hatano, K. Takahashi, and H. Tokumoto, Journal of Vacuum Science & Technology B **13**, 1095 (1995).
[28] B. Gilbert, B. H. Frazer, A. Belz, P. G. Conrad, K. H. Nealson, D. Haskel, J. C. Lang, G. Srajer, and G. D. Stasio, Journal of Physical Chemistry A **107**, 2839 (2003).
[29] R. Laskowski and P. Blaha, Physical Review B **82**, 205104 (2010).
[30] P. Krüger, Journal of Physics: Conference Series **190**, 012006 (2009).
[31] P. Krüger, Phys. Rev. B **81**, 125121 (2010).
[32] S. Valencia, Z. Konstantinovic, A. Gaupp, D. Schmitz, L. Balcells, and B. Martínez, Journal of Applied Physics **109**, 07D718 (2011).
[33] L. Samet, D. Imhoff, J.-L. Maurice, J.-P. Contour, A. Gloter, T. Manoubi, A. Fert, and C. Colliex, The European Physical Journal B - Condensed Matter and Complex Systems **34**, 179 (2003), 10.1140/epjb/e2003-00210-8.
[34] J. A. Mundy, L. Fitting Kourkoutis, Y. Hikita, T. Hidaka, H. Y. Hwang, and D. A. Muller, Microscopy and Microanalysis **16**, 1398 (2010).
[35] N. Wang, H. Chen, H. He, W. Norimatsu, M. Kusunoki, and K. Koumoto, Scientific Reports **3**, 3449 (2013).
[36] N. Nagakawa, H. Y. Hwang, H. Y., and D. A. Muller, Nature Materials 5, 204 (2006).
[37] H. H. Boschker, J. Verbeeck, R. Egoavil, S. Bals, G. van Tendeloo, M. Huijben, E. P. Houwman, G. Koster, D. H. A. Blank, and G. Rijnders, Advanced Functional Materials **22**, 2235 (2012).
[38] J. A. Mundy, Y. Hikita, T. Hidaka, T. Yajima, T. Higuchi, H. Y. Hwang, D. A. Muller, and L. F. Kourkoutis, Nature Communications (2014), 10.1038/ncomms4464.
[39] A. Monsen, F. Song, Z. Li, J. Boschker, T. Tybell, E. Wahlstr/"om, and J. Wells, Surface Science **606**, 1360 (2012).
[40] M. Huijben, L. W. Martin, Y.-H. Chu, M. B. Holcomb, P. Yu, G. Rijnders, D. H. A. Blank, and R. Ramesh, Phys. Rev. B **78**, 094413 (2008).
[41] J. Garcia-Barriocanal, J. Cezar, F. Bruno, P. Thakur, N. Brookes, C. Utfeld, A. Rivera-Calzada, S. Giblin, J. Taylor, J. Duffy, S. Dugdale, T. Nakamura, K. Kodama, C. Leon, S. Okamoto, and J. Santamaria, Nature Communications (2010), 10.1038/ncomms1080.
[42] J. D. Burton and E. Y. Tsymbal, Physical Review B **80**, 174406 (2009).

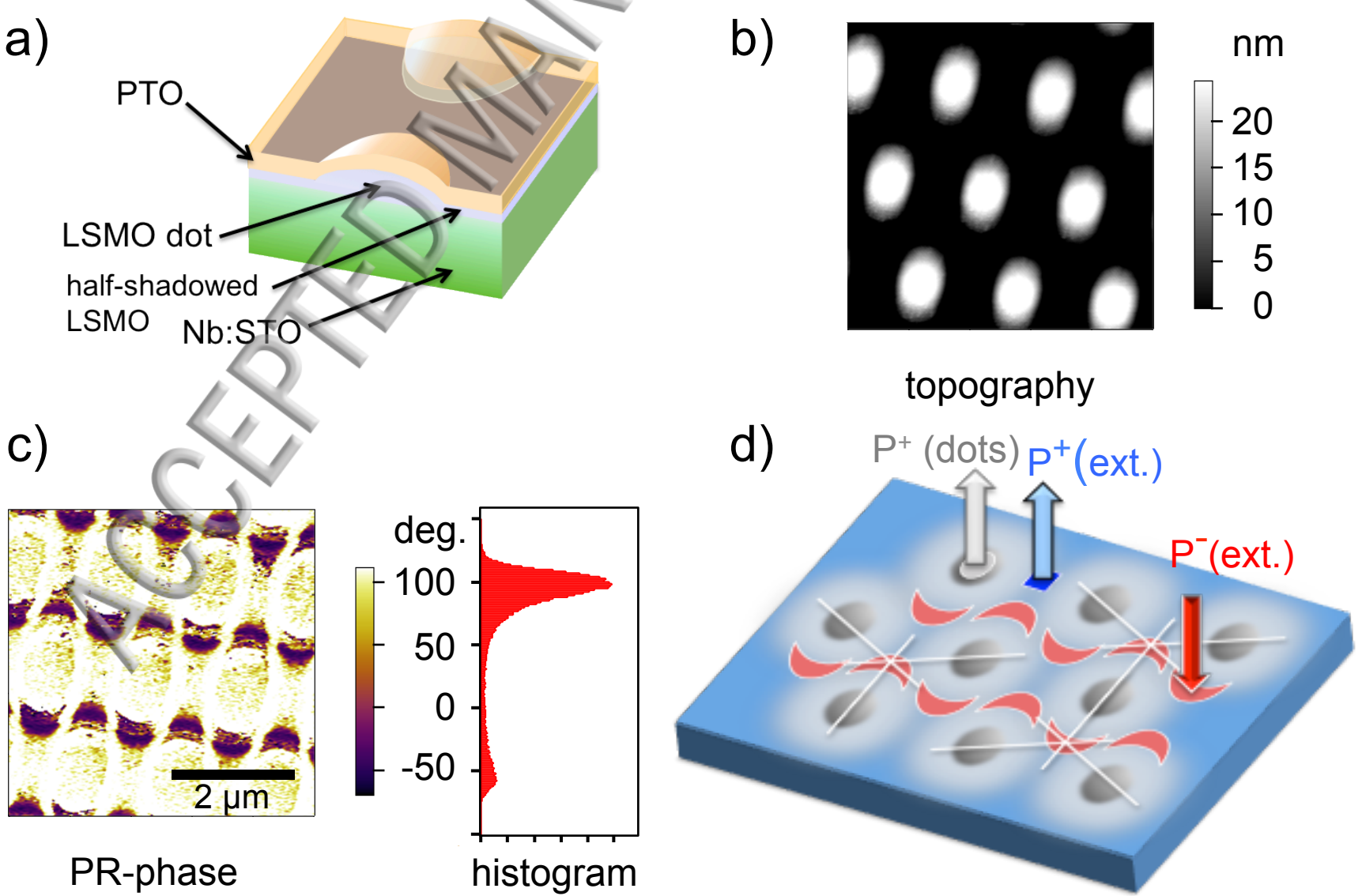

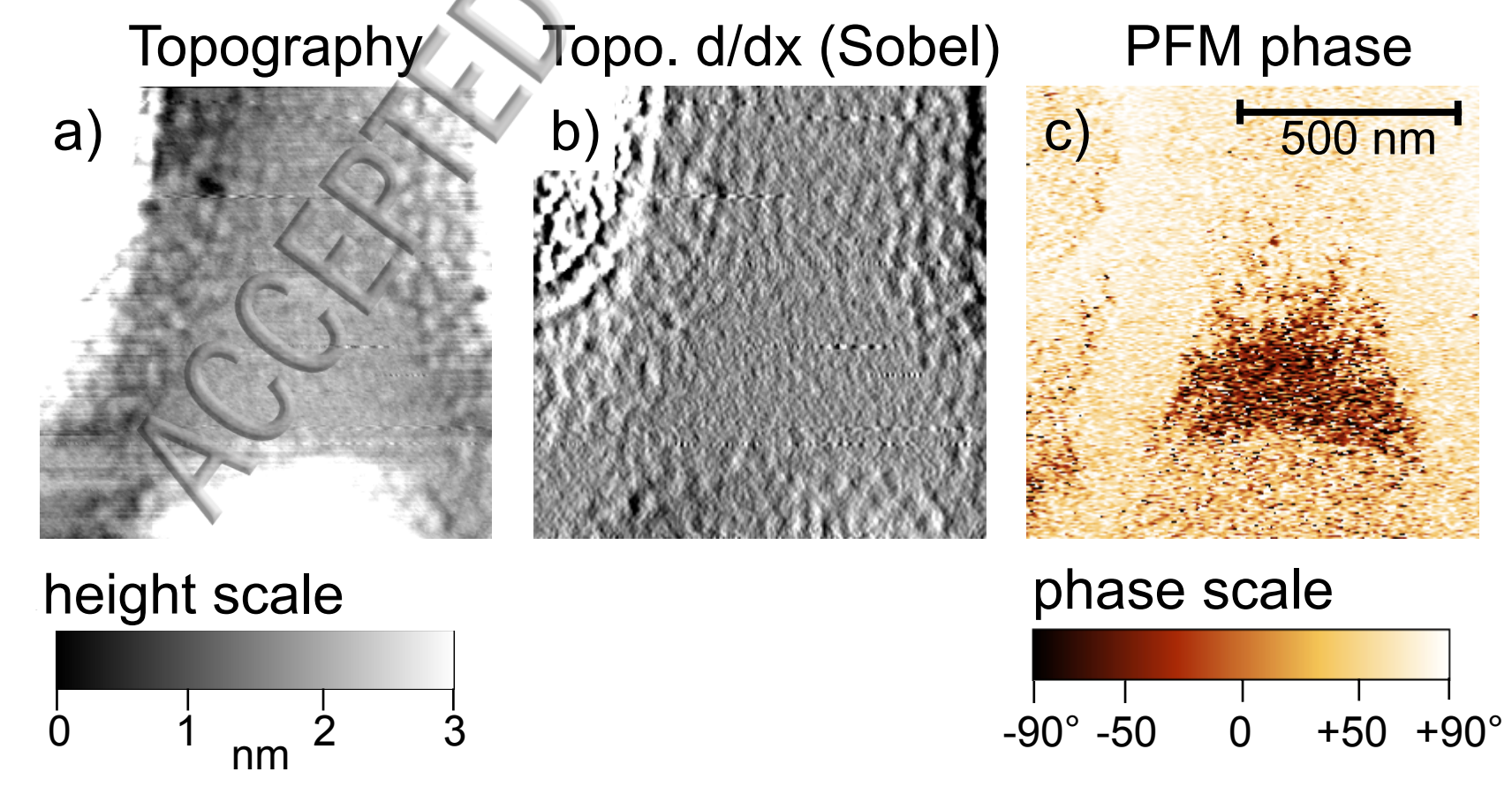
Topography
Topo. d/dx (Sobel)
PFM phase
a)
b)
c)
500 nm
ACCEPTED
height scale
0
1
2
3
nm
phase scale
-90°
-50
0
+50
+90°

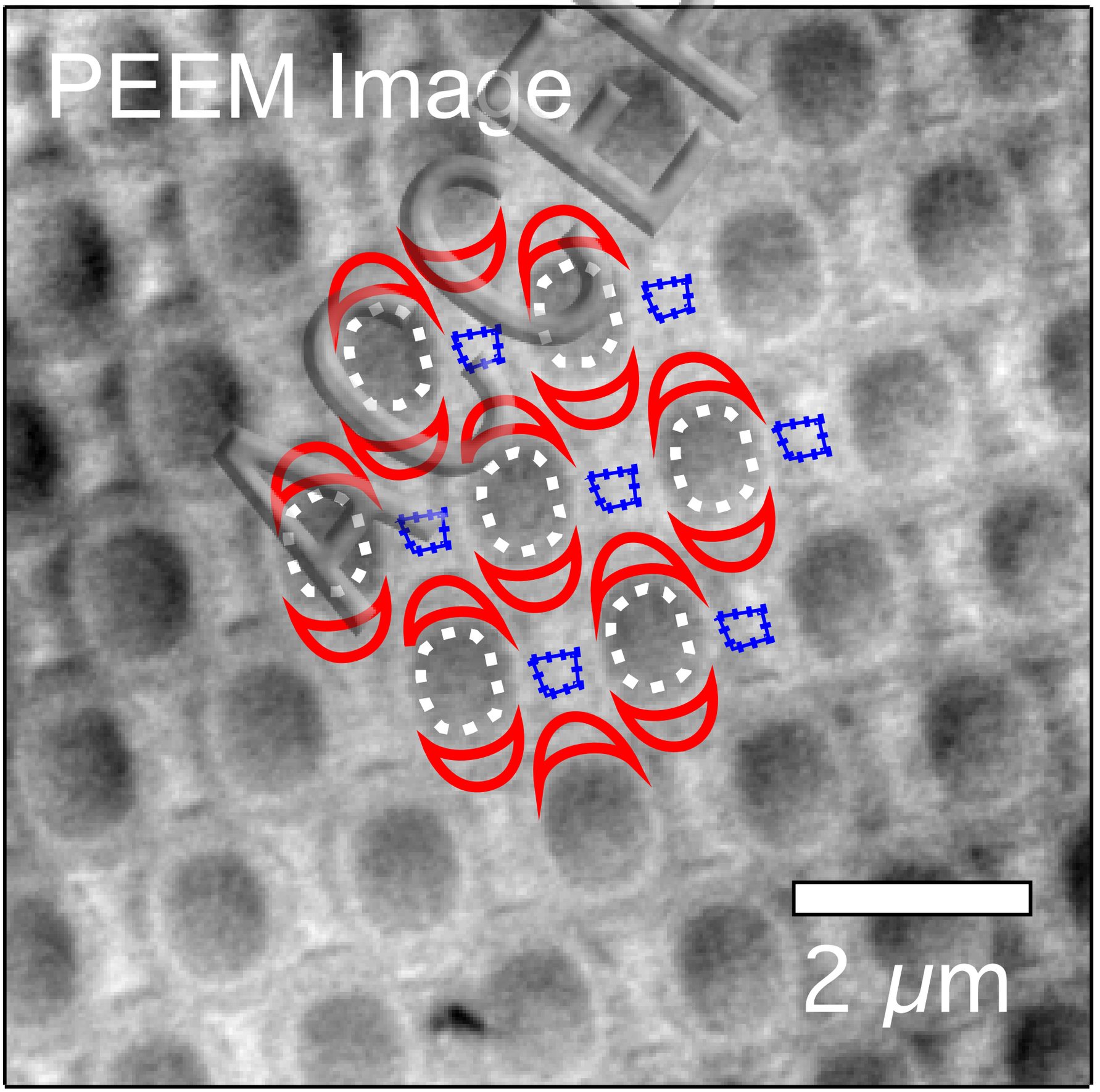
PEEM Image
2 μm